Neuron 52, 871–882, December 7, 2006 ©2006 Elsevier Inc. DOI 10.1016/j.neuron.2006.10.023

Integration and Segregation of Activity in Entorhinal-Hippocampal Subregions by Neocortical Slow Oscillations

Yoshikazu Isomura,[1,2,3,5] Anton Sirota,[1,5] Simal Özen,[1] Sean Montgomery,[1] Kenji Mizuseki,[1] Darrell A. Henze,[1,4] and György Buzsáki[1,*]

[1] Center for Molecular and Behavioral Neuroscience
Rutgers, The State University of New Jersey
197 University Avenue
Newark, New Jersey 07102

[2] Neural Circuit Theory
RIKEN Brain Science Institute
2-1 Hirosawa, Wako
Saitama 351-0198
Japan

[3] System Neuroscience
Tokyo Metropolitan Institute for Neuroscience
2-6 Musashidai, Fuchu
Tokyo 183-8526
Japan

[4] Neuroscience Drug Discovery
Merck Research Laboratories
770 Sumneytown Pike, WP44E-200
West Point, Pennsylvania 19486

Summary

Brain systems communicate by means of neuronal oscillations at multiple temporal and spatial scales. In anesthetized rats, we find that neocortical "slow" oscillation engages neurons in prefrontal, somatosensory, entorhinal, and subicular cortices into synchronous transitions between UP and DOWN states, with a corresponding bimodal distribution of their membrane potential. The membrane potential of hippocampal granule cells and CA3 and CA1 pyramidal cells lacked bimodality, yet it was influenced by the slow oscillation in a region-specific manner. Furthermore, in both anesthetized and naturally sleeping rats, the cortical UP states resulted in increased activity of dentate and most CA1 neurons, as well as the highest probability of ripple events. Yet, the CA3-CA1 network could self-organize into gamma bursts and occasional ripples during the DOWN state. Thus, neo/paleocortical and hippocampal networks periodically reset, self-organize, and temporally coordinate their cell assemblies via the slow oscillation.

Introduction

The mammalian cortex is traditionally divided into neocortex (isocortex), paleocortex, and archicortex (hippocampus) and their subdivisions on the basis of cellular architectonics and connectivity patterns (MacLean, 1990). However, the physiological mechanisms that allow segregation and integration of neuronal information in the highly interconnected cortical-hippocampal networks (Sporns et al., 2000) are poorly understood. One hypothesis is that the spatial extent of neuronal recruitment and the direction of activity flow are controlled by a large family of neuronal oscillators (Buzsaki and Draguhn, 2004). Because the dominance of particular cortical oscillations is controlled by brain state and the animal's behavior (Steriade and Buzsáki, 1990; McCormick, 1992; Buzsaki and Draguhn, 2004), it is expected that the functional boundaries of cooperative ensemble activity are determined by the particular constellations of oscillators at any given moment (Buzsaki, 1996; Friston, 2000; Sirota et al., 2003; Pelletier et al., 2004).

In the neocortex, deep slow wave sleep is characterized by widespread synchronized oscillatory patterns, defined primarily by spatially coherent delta waves (Achermann and Borbely, 1997). Neocortical delta waves represent transient (200–500 ms) cessation of synaptic and spiking activity of both principal cells and interneurons of all cortical layers, followed by episodes (0.3–1 s) of sustained activity (Steriade and Buzsáki, 1990; Battaglia et al., 2004). Similarly, under anesthesia, silent and active periods alternate regularly, giving rise to "slow" oscillation (0.5–1.5 Hz) (Steriade et al., 1993a, 1993b, 1993c; Amzica and Steriade, 1995; Destexhe et al., 1999). Intracellularly, the active and silent periods of network patterns, respectively, correspond to plateau depolarization, associated with subthreshold oscillations, intense synaptic barrages, and spiking activity (UP state) and hyperpolarized quiescence or disfacilitation (DOWN state), both under anesthesia (Steriade et al., 1993b; Cowan and Wilson, 1994) and natural slow wave sleep (Timofeev et al., 2001; Petersen et al., 2003). Although slow oscillations can also be observed in the thalamus (Hughes et al., 2002) and the basal ganglia (Wilson and Kawaguchi, 1996), it is regarded as an intrinsic neocortical pattern because it not only survives after surgical isolation of a slab of neocortex from its thalamocortical and subcortical inputs (Timofeev et al., 2000) but also persists in a small piece of neocortical tissue in vitro (Sanchez-Vives and McCormick, 2000; McCormick et al., 2003; Shu et al., 2003; Cunningham et al., 2006). The mechanisms that govern UP and DOWN states of neurons may include network-level excitatory-inhibitory mechanisms (Steriade et al., 1993b; McCormick et al., 2003) and intrinsic properties of the constituent neurons (Cowan and Wilson, 1994; Amzica and Steriade, 1995; Wilson and Kawaguchi, 1996; Sanchez-Vives and McCormick, 2000; Cunningham et al., 2006).

Here we utilize the alternation between synchronous activity and silent periods in the neocortex (Steriade et al., 1993c; Amzica and Steriade, 1995; Achermann and Borbely, 1997; Battaglia et al., 2004) as unique temporal windows to examine how neocortical, paleocortical (parahippocampal), and hippocampal networks integrate and segregate the activity of their neurons without the disadvantage of surgical or pharmacological manipulations. Do synchronous neocortical patterns associated with slow oscillations invade and affect all parahippocampal and hippocampal subregions equally

*Correspondence: buzsaki@axon.rutgers.edu
[5] These authors equally contributed to the work.

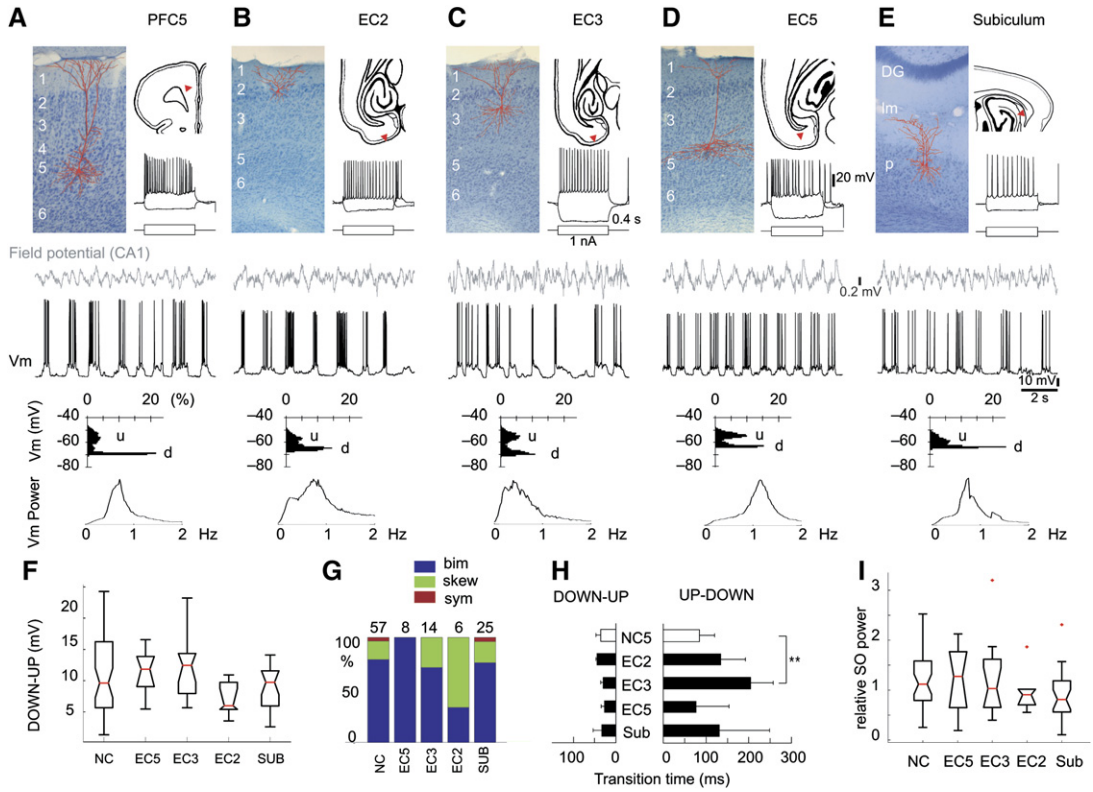

Figure 1. Membrane Potential Bimodality in Neocortical and Paleocortical Neurons

(A–E) (Top) Morphology, somatic location, and current-induced responses of intracellularly recorded principal neurons in prefrontal layer 5 (PFC5), entorhinal layers 2, 3, and 5 (EC2, 3, 5), and subicular neurons. Cortical layers 1 to 6 are shown. DG, dentate gyrus; lm, str. lacunosum-moleculare; p, pyramidal layer. (Middle) Membrane potential (Vm) in each illustrated neuron. Histograms, distribution of the membrane potential. Note bimodal distribution (UP, u; DOWN, d) of the potential. (Bottom) Spectral power of membrane potential in each neuron. Note peak at 0.6–1 Hz.

(F) Magnitude of DOWN-UP shift of membrane potential in neocortical (NC), entorhinal (EC), and subicular (Sub) neurons. Box plot, each box encloses data between the first and third quartile with the median value in red. Whiskers extending from the box mark the rest of the data.

(G) Distribution of subgroups (bimodal, bim; skewed, skew; symmetric, sym). Numbers of neurons in each subgroup are indicated on top.

(H) DOWN-UP (onset to half-amplitude) and UP-DOWN (half-amplitude to DOWN) transition times in the neuron groups. Error bars display SEM.

(I) Relative power of intracellular slow oscillation (SO; 0.5–1.5 Hz). Same display as in (F).

(Siapas and Wilson, 1998; Sirota et al., 2003; Battaglia et al., 2004; Pelletier et al., 2004)? Are these subregions controlled by neocortical inputs or can they support independent, self-organized gamma and ripple oscillations (Buzsaki et al., 1992; Bragin et al., 1995) in the absence of neocortical inputs? To address these questions, we simultaneously recorded and analyzed local field potentials and extracellular unit activity in one cortical area and intracellular activity in another cortical area in anesthetized rats, as well as local field potentials and extracellular unit activity in cortical and hippocampal regions in naturally sleeping rats.

Results

Bimodality of Membrane Potential in Neo- and Paleocortical Neurons

In 108 rats, we obtained stable intracellular recordings from neurons from the neocortex (prefrontal, n = 34; somatosensory, n = 22; visual n = 3) and paleocortex (entorhinal cortex, n = 27; subiculum, n = 26) with simultaneous local field potential (LFP) recordings from hippocampal CA1 pyramidal layer or from multiple sites in the CA1-dentate gyrus axis (n = 17) or, in some cases (n = 7), in the neocortex or entorhinal cortex. All but the somatosensory neurons have been identified morphologically following intracellular injection of biocytin. In the absence of hippocampal theta oscillations (Buzsaki, 1996), neocortical and paleocortical neurons showed a prominent slow oscillation (0.5–1.5 Hz), consisting of alternating depolarized UP states with spikes and hyperpolarized DOWN states, resulting in a bimodal distribution of the membrane potential (Figures 1A–1E and see Figure S1 in the Supplemental Data available online), confirming and extending previous observations both in vivo and in vitro (Steriade et al., 1993b, 1993c; Sanchez-Vives and McCormick, 2000; McCormick et al., 2003; Shu et al., 2003; Dickson et al., 2003; Cunningham et al., 2006). The duration of the UP and DOWN states alternated relatively regularly, giving rise to a peak power between 0.5 and 1.5 Hz (Figures 1A–1E, 1I, and Figure S1).

Similar to neocortical cells, principal neurons in both superficial (layer 2, n = 6; layer 3, n = 14) and deeper (layer 5, n = 8) layers of the entorhinal cortex (Figures 1B–1D) and the subicular pyramidal cells (Figure 1E;

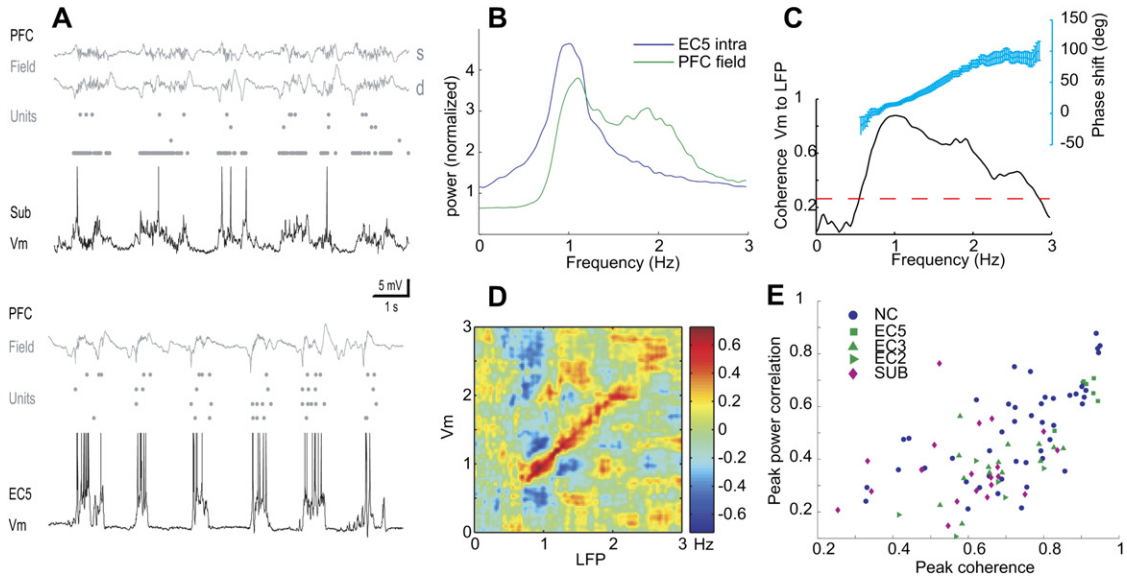

Figure 2. Coherent Slow Oscillations in Neocortex and Paleocortex

(A) Field potential recordings in superficial (s) and deep (d) layers of the prefrontal cortex (PFC; dots, unit discharges) and intracellular activity in a subicular neuron. (Bottom) Similar recording with a layer 5 entorhinal cell (EC5).

(B) Normalized power of the field and intracellular activity for the recordings in (A) (bottom).

(C) Coherence and phase shift (blue inset, error bars represent 95% confidence interval) between field and intracellular membrane potential. Dotted line, $p = 0.05$.

(D) Correlation ("comodulation") between power in the field and intracellular membrane potential.

(E) Relationship between coherence and comodulation of power at the frequency of slow oscillation for neocortical, entorhinal, and subicular neurons.

n = 25) and one subicular interneuron displayed spontaneous alternations in their membrane potential between UP and DOWN state. During the UP state, neurons showed robust fast oscillations in the membrane voltage (20–70 Hz; gamma range), and one or several spikes per UP episode were triggered by the peaks of the fast oscillation. However, their firing rates during the slow oscillation periods (UP and DOWN states combined) were not, on average, significantly different from the firing rates during hippocampal theta periods (Table S1). Current injection-induced hyperpolarization of the membrane prevented the occurrence of the spikes but not gamma oscillations. During the DOWN states spiking was rarely observed, and fast oscillations were either absent or significantly less than in the UP state. The above observations suggest that, similar to the neocortex, UP states of entorhinal and subicular neurons during slow oscillations are determined primarily by network-generated synaptic mechanisms.

Quantitative assessment showed that the distribution of the membrane potential values was either bimodal or skewed in almost all neurons in the neocortex and paleocortex, with a large variance in the UP and small variance in the DOWN states (Figure 1G). The voltage difference between UP and DOWN states was smallest in layer 2 stellate/pyramidal cells of the entorhinal cortex, but, in pyramidal neurons of layers 3 and 5 and subiculum, the potential fluctuation was comparable to that of the neocortical cells (Figure 1F). The transition from DOWN to UP states was sharp and similar in all neurons. However, the UP to DOWN transition was significantly slower in entorhinal layer 3 neurons than in the other cell types (Figure 1H; $p < 0.01$; ANOVA and Duncan's multiple range test). Similar to neocortical neurons UP and DOWN states alternated rhythmically (Figure 1I).

Coherent Slow Oscillations in the Neo- and Paleocortical Networks

The widespread nature of the slow oscillation was demonstrated by the robust synchrony of activity between structures. DOWN states could be recognized visually by the hyperpolarized membrane potential in intracellular recordings and by positive going local field potentials in deep layers associated with a reduction of fast activity and the absence or extreme paucity of extracellularly recorded spikes. In contrast, UP states were associated with fast activity in both intracellular recordings and local field potentials (Steriade et al., 1993b; Mukovski et al., 2006). Simultaneous intracellular and extracellular recordings from various cortical locations showed that UP-DOWN fluctuations occurred coherently across virtually the entire neocortex, entorhinal cortex, and subiculum (Figure 2 and Figure S3). Prominent membrane potential fluctuations in a single neuron reliably correlated with the population patterns of the extracellularly recorded units and field potentials of a distant structure (Figure 2A). These observations were quantified by analyses in the frequency domain. Spectral power of both LFP and intracellular potential showed peaks between 0.5–1.5 Hz (Figure 2B). Coherence values were largest at the frequency of peak power of the slow oscillation (Figure 2C). The magnitude of phase difference between field and intracellular potential increased linearly with frequency for most neurons, indicating that fixed time delays determine the magnitude of phase shift between the respective oscillations. In

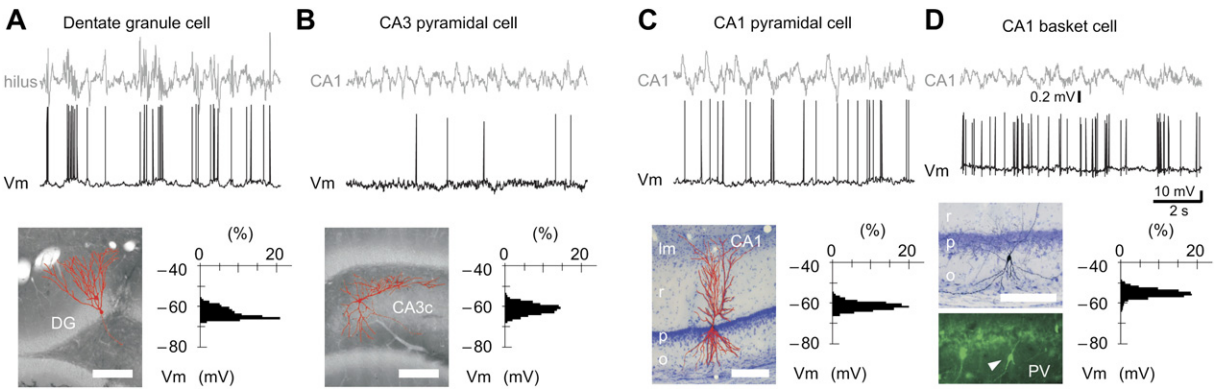

Figure 3. Lack of Membrane Potential Bimodality in Hippocampal Neurons

(A–D) Same layout as in Figure 1. lm, str. lacunosum-moleculare; r, str. radiatum; p, pyramidal layer; o, str. oriens. Fluorescent photograph (D) shows parvalbumin-immunoreactivity (PV) of the basket neuron.

addition to coherence between the intracellular and extracellular signals, the strongest correlation between the power fluctuations of LFP and the intracellular signal was also confined to the slow oscillation band (Figure 2D). For group comparison, the extracellular recording site in the CA1 pyramidal layer was used for the assessment of neocortical slow oscillation (see justification below). The highest phase and power correlation with the LFP was observed in neocortical neurons and layer 5 entorhinal cells, followed by superficial entorhinal and subicular neurons (Figure 2E; see also Figure S2).

Absence of Membrane Potential Bimodality in Hippocampal Neurons

To compare the behavior of membrane potential of neocortical cells with that of hippocampal neurons, we examined intracellular activity of hippocampal neurons in an additional 106 rats. All recorded neurons were morphologically identified. In contrast to the robust bimodal distribution of the membrane potential in neocortical, entorhinal, and subicular neurons, prominent voltage fluctuation of the membrane potential was not present in hippocampal pyramidal neurons during cortical slow oscillations (Figure 3), and bimodality was present in only one CA3 neuron. Five of the eight granule cells, 28 of the 58 CA1, and 12 of the 41 CA3 pyramidal cells had skewed membrane potential distribution, whereas, in the remaining principal neurons and a single CA1 basket cell, the distribution of membrane potential values was unimodal and symmetric (Figures 3A–D). Fast activity, reflecting mostly synaptic inputs, was almost continuously present, in contrast to the regular alternation of "noisy" and "quiescent" epochs in neocortical, entorhinal, and subicular neurons.

Modulation of Hippocampal Circuits by Slow Oscillations

Although no bimodality of the membrane potential was observed in intracellular (somatic) recordings of hippocampal neurons during cortical slow oscillations, the slow oscillation-related synchronous discharge of entorhinal neurons may nevertheless impose a detectable effect on the hippocampal network. To examine this hypothesis, we monitored the laminar distribution of currents in the hippocampus, triggered by the DOWN-UP transitions of the intracellular membrane potential in entorhinal cortical neurons (n = 14 rats). The depth position of the recording electrodes in the CA1-dentate axis was calibrated by stimulus-evoked potentials in response to perforant path or commissural path stimulation and by the spontaneously occurring sharp waves. Current-source density (CSD) analyses of these events precisely identify the various cell body and dendritic layers in the hippocampus (Ylinen et al., 1995) (Figures 4A and 4B). The largest current sink, associated with the DOWN-UP shift, occurred in the str. lacunosum-moleculare in all rats (Wolansky et al., 2006; Klooster-man, 2003). In 8 of the 14 experiments, an additional sink was also present in the dentate molecular layer (e.g., Figure 4C), indicating excitatory synaptic activation of hippocampal neurons by the DOWN-UP shifts in entorhinal layer 2 and 3 cells (Amaral and Witter, 1989). The rhythmic nature of excitatory drive was quantified using coherence analysis between LFP at multiple hippocampal locations and the intracellular signal in each experiment (Figure 4D). For the representation of group data, principal component analysis was performed on the depth profiles of coherence at the frequency of slow oscillation across all animals (see Experimental Procedures). The depth profile of the first component likely reflected the contribution of volume-conduced currents produced by slow oscillation in neocortical circuits (see also Figure 2E) (Steriade et al., 1993a). The peak of the second component corresponded to the rhythmic sink locations in the molecular layer and str. lacunosum-moleculare, the target layers of the entorhinal inputs (Figure 4E).

Volume conduction of the potentials associated with neocortical slow oscillations to the hippocampus was exploited to relate the activity of intracellularly recorded neurons (n = 137) of different brain structures and separate animals to a common reference, i.e, the phase of slow oscillation derived from LFP in the CA1 pyramidal layer. LFP in the CA1 pyramidal layer reliably reflected volume-conducted slow oscillations generated in the neocortex as shown by the uniform phase (~180 degrees) of DOWN-UP transition of the intracellular membrane potential of neocortical cells (Figure S3). Superficial entorhinal cortical cells and subicular neurons, on

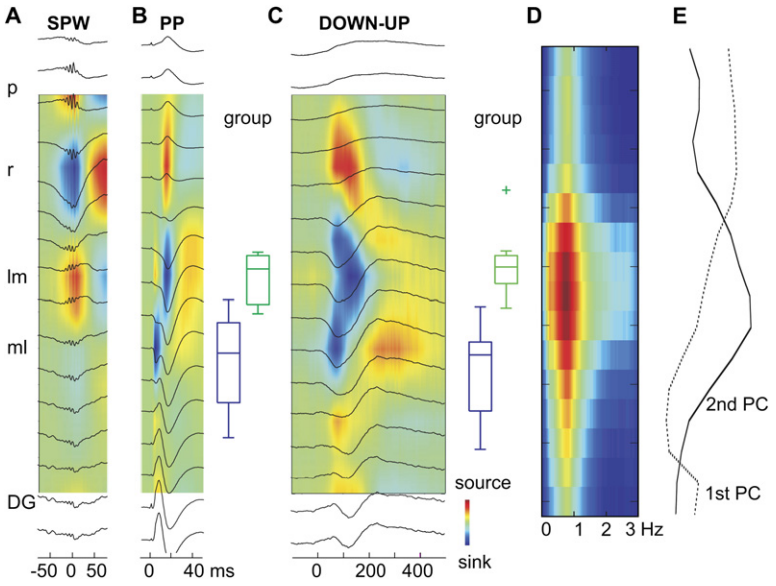

Figure 4. UP State-Related Excitation of Hippocampal Neurons

(A) Ripple-triggered field potentials (line traces simultaneously recorded at 100 μm intervals) and current-source density (CSD) plot identify the sharp wave generated sink in str. radiatum.

(B) Perforant path (PP) stimulation-evoked field response and CSD. Note sinks in the molecular layer (ml) and str. lacunosum-moleculare (lm). Box plots, group data of sink maxima positions (green, lm ; blue, ml; n = 14 rats). The site with the maximum amplitude ripple (CA1 pyramidal layer) served to align depth recording sites across experiments.

(C) Averaged hippocampal field traces and CSD, triggered by DOWN-UP transitions in a layer 3 entorhinal neuron (see Figure S9 for a similar plot in naturally sleeping rat).

(D) Depth profile of the coherence between intracellular membrane potential and the LFP in hippocampus in the slow oscillation frequency range.

(E) Group (n = 14) representation of the coherence (as in [D]) by principal component analysis. Depth profiles of first (dotted line) and second (solid line) principal components (PC) of peak coherence depth profiles aligned to the CA1 pyramidal layer in each experiment. x axis, arbitrary units. Note wide peak of the second PC corresponding to depth locations of str. lacunosum-moleculare and molecular layer.

average, were phase shifted by approximately 60° relative to neocortical and layer 5 entorhinal neurons, corresponding to a 150–200 ms time delay (Figure S3). The phase shift was similar in layer 2 and layer 3 neurons. Although hippocampal pyramidal cells did not display bimodal membrane potential distribution, the CSD analysis suggested that pyramidal cells nevertheless were affected by the cortical slow oscillation.

To uncover the relationship between membrane potential of hippocampal neurons and the phasic modulation of slow oscillation, we analyzed the joint probability density function (JPDF) of the membrane potential of individual neurons and the phase of the slow oscillation (Figure S4). This analysis showed that the membrane potential of all neocortical, paleocortical, and most CA1 hippocampal cells is indeed biased by the phase of the slow oscillations (Figure 5A; see also Figure S4 for raw membrane potential). In contrast to neo/paleocortical neurons, the maximum relative depolarization of most CA3 cells coincided with the neocortical DOWN state. The phase relation of individual CA1 neurons varied across the entire cycle, suggesting that some may respond preferentially to the entorhinal input whereas others to the phase-shifted CA3 neurons. The slow oscillation-related intracellular activity of granule cells could not be examined because in those experiments the extracellular electrode was placed in the CA3-hilar region rather than the CA1 pyramidal layer.

To further investigate the phase relationship between slow oscillations and neuronal activity in the CA3-CA1 regions and dentate area, we examined the firing patterns of the extracellularly recorded and isolated principal cells and putative interneurons (n = 946 units in n = 137 rats). Analysis of individual units revealed three broad classes of CA1 units, preferentially active during UP, DOWN, or both states (Figure 5 and Figure S5). Although the proportions of neurons in each class may have been affected by the level of anesthesia, units representing different classes were observed on the same electrode (Figures 5B–5D). In-phase and anti-phase firing preferences were also observed in putative CA1 interneurons (Figure 5B). In the subset of animals implanted with silicon probes (n = 17), units were also recorded in the CA3 region and/or dentate gyrus. Neurons in the dentate region were preferentially active during the UP state of slow oscillation, whereas most CA3 units discharged preferentially during the DOWN state (Figures 5C–5E). In accordance with the membrane potential analysis of the intracellularly recorded cells, these findings are compatible with the hypothesis that, during the neocortical UP state, CA1 neurons are driven either directly by the layer 3 entorhinal input or by the dentate-CA3-CA1 trisynaptic pathway, whereas, in the DOWN state, the self-organized activity in the CA3 region is their main driving force.

Periodic Reset of Neo-, Paleocortical, and Hippocampal Activity during Natural Sleep

To examine to what extent the modulatory effects of slow oscillation on hippocampal activity is due to the effect of anesthesia, we reexamined many aspects of the above experiments in naturally sleeping rats (n = 9). DOWN states and concurrent delta waves in the neocortex were associated with cessation of neuronal activity in the neocortex, entorhinal cortex, and the dentate gyrus (Figure 6). Similar to the observations under anesthesia, the majority of CA3 neurons showed an enhanced discharge probability at times when the entorhinal input was silent (Figure 6A). The majority of CA1 neurons fired during the UP state, but a significant number of cells preferred to discharge during the DOWN state, likely driven by the synchronous activity of CA3 neurons. The similarity of the patterns between anesthesia and sleeping is further supported by the preserved phase relations of dentate and CA3 neurons in the same animal (Figure S6).

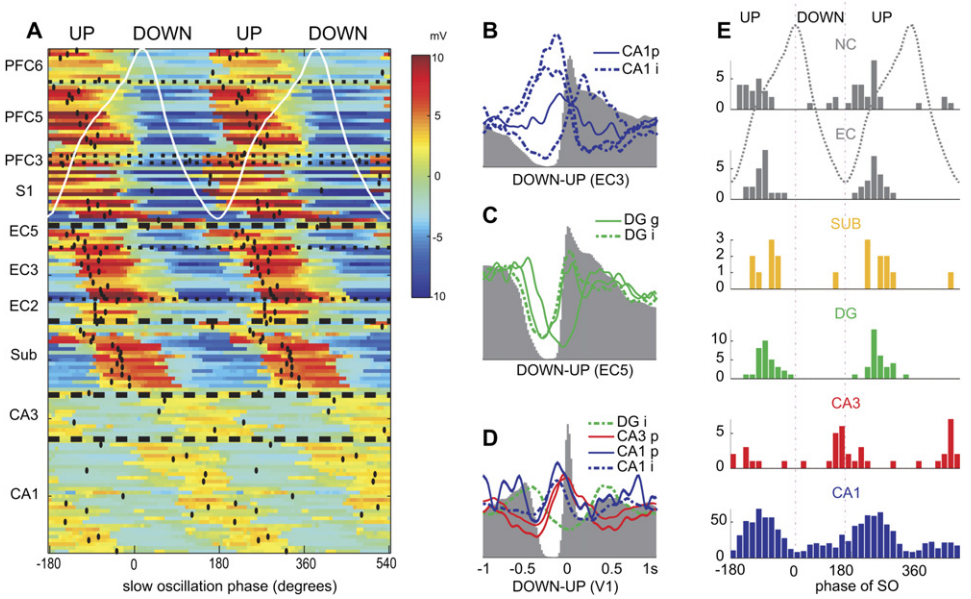

Figure 5. Neo/Paleocortical Input-Dependent and -Independent Activity of Hippocampal Neurons during Anesthesia

(A) Group representation of the slow oscillation-related modulation of distribution of the membrane potential. Each line corresponds to a single intracellularly recorded neuron (n = 137). Color code, magnitude of the most likely values of the membrane potential, beyond what is expected from independence, for each phase (Figure S4; red, relatively depolarized from the mean). White trace, averaged field trace from CA1 pyramidal layer, aligned to phase axis. PFC, prefrontal cortex (layers 6, 5, and 3); S1, somatosensory cortex; EC, entorhinal cortex; Sub, subiculum. Note the anti-phase activity of most CA3 pyramidal cells and wide phase preference of CA1 neurons.

(B–D) Examples of cross-correlograms of single hippocampal neurons, referenced to the DOWN-UP state transition in entorhinal (EC3, EC5) and neocortical (NC) neurons (gray histograms). Note opposite phase preference of simultaneously recorded units. p, pyramidal cell; g, putative granule cell, i, putative interneuron.

(E) Distribution of preferred discharge phases of single neurons (intracellular and extracellular recordings combined) in various regions. Only neurons that were significantly modulated by slow oscillation are shown (n = 643 of 946 cells; n = 130 animals). Note that most CA3 and a portion of CA1 neurons discharge preferentially in the DOWN state, whereas nearly all DG cells discharge preferentially during the UP state.

Neo-, Paleocortex-Dependent, and -Independent Gamma Oscillations in the Hippocampus

The apparent slow oscillation-modulated depolarizations in single hippocampal neurons suggest that hippocampal network activity is also modulated by the slow oscillation. Gamma frequency power in the neocortex is known to be modulated by slow oscillations in all layers (Steriade et al., 1993b; Hasenstaub et al., 2005; Mukovski et al., 2006). In contrast, gamma power in the hippocampus varied as a function of both depth and phase of slow oscillation. Maximum gamma power in the dentate gyrus and CA1 str. radiatum sometimes alternated in phase (Figure 7A), suggesting that prominent gamma oscillation epochs in str. radiatum can emerge

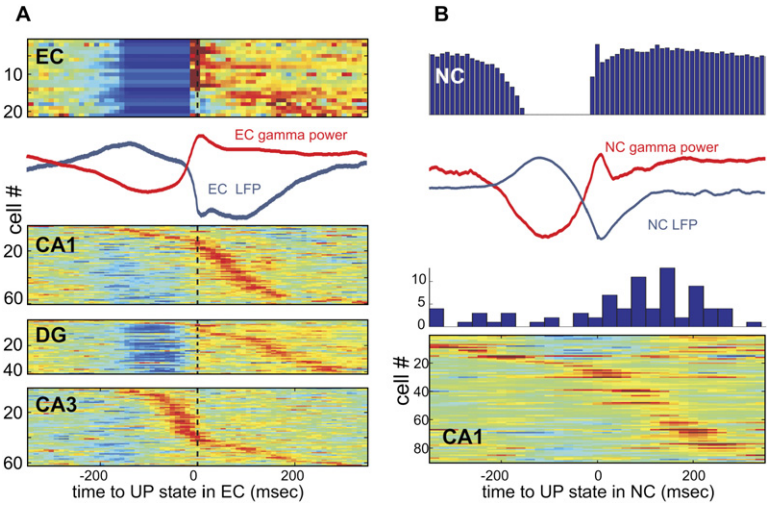

Figure 6. Neo/Paleocortical Input-Dependent and -Independent Activity of Hippocampal Neurons during Natural Slow Wave Sleep

(A) Activity in the entorhinal cortex and hippocampus relative to the onset of the UP state in the entorhinal cortex (time zero in all plots). From top to bottom: color-coded stacked cross-correlograms of EC neurons, average LFP (layer 5; blue) and gamma power (red) in EC, color-coded stacked cross-correlograms of DG, CA1, and CA3 neurons (recorded in separate sleep sessions). Each line is a single neuron. Data are from a single rat. Note that firing pattern distributions are similar to those observed under anesthesia (Figure 5).

(B) Group data for the slow oscillation-related firing patterns of CA1 neurons. DOWN-UP transitions were determined by the population firing patterns of simultaneously recorded neocortical neurons (NC). Traces, average LFP (blue) and gamma power (red) in the neocortex. Color-coded histogram (bottom), stacked cross-correlograms of 89 significantly correlated CA1 cells (n = 8 rats) sorted by time lag of their peaks. Blue histogram, distribution of the time lags of cross-correlogram peaks of CA1 neurons relative to the UP state. Note that the majority of CA1 cells fire preferentially in the UP state.

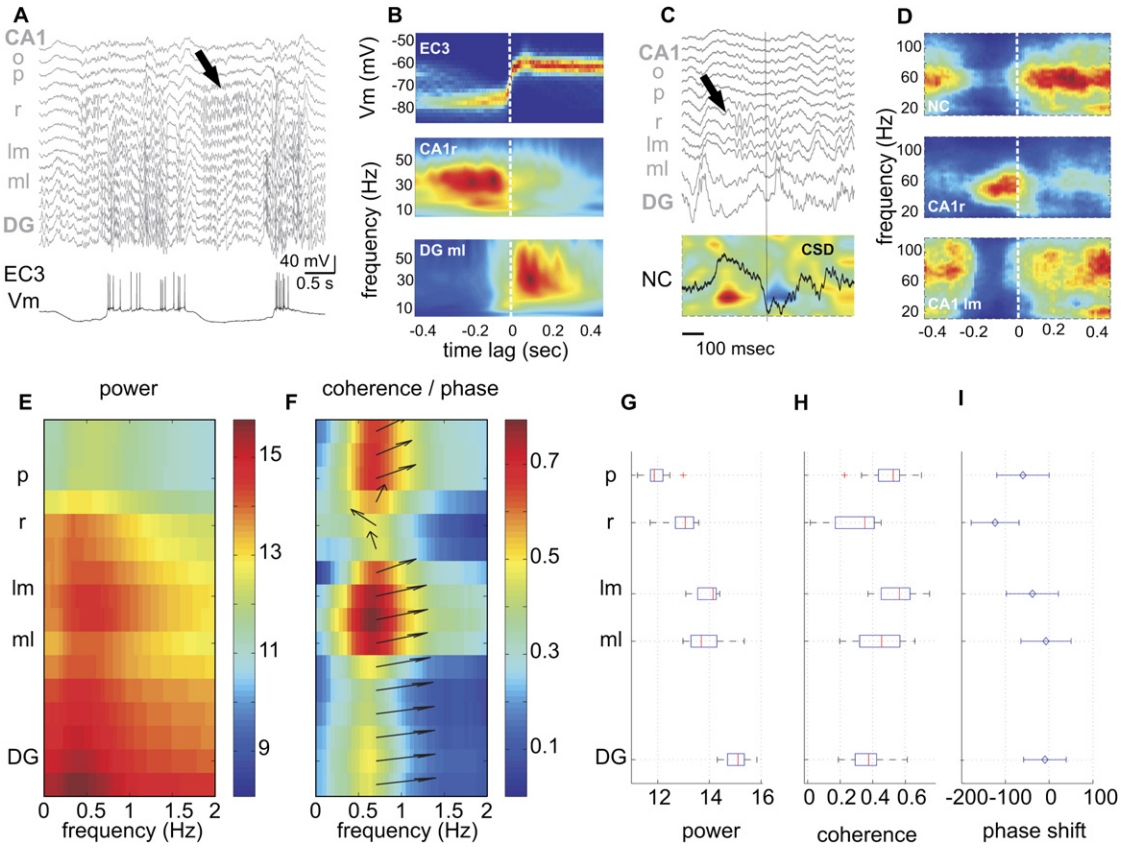

Figure 7. Slow Oscillation Phase and Layer Dependence of Hippocampal γ Oscillation

(A) Multisite local field recording in the hippocampus and intracellular trace from an entorhinal layer 3 neuron (EC3) during anesthesia.

(A, B, E, and F) Data from the same rat.

(B) Distribution of the membrane potential (top) and average spectrogram of the local field potential in str. radiatum (middle) and molecular layer (bottom) triggered by DOWN-UP transitions (n = 2298 epochs). Note increased gamma power in str. radiatum during the DOWN state and in the molecular layer during the UP state.

(C and D) Data from natural sleep. (C) Multisite LFP recording in the hippocampus (traces, top) and CSD map (bottom) from the neocortex (NC; bottom panel). LFP trace in NC is from layer 5. Note train of gamma oscillation in str. radiatum (black arrow) during the DOWN state of the neocortex (source, red). (D) Average spectrograms of LFP in NC, CA1 str. radiatum (CA1r) and lacunosum-moleculare (CA1lm) triggered by the onset of activity following the delta wave (n = 98 events). Note similar patterns to (A) and (B).

(E) Spectral power in the 0–2 Hz frequency range of the integrated gamma power (25–60 Hz) at 16 recording sites.

(F) Coherence between integrated gamma power at each site and intracellular membrane potential. Arrows, phase shift between membrane potential and gamma power at peak frequency (0.6 Hz). Note low coherence and opposite preferred phase of gamma power in str. radiatum.

(G–I) Group results for power, coherence (box plots) and phase (circular mean ± SD) (n = 14 anesthetized rats).

also during neocortical-entorhinal DOWN state. The average spectrograms of the LFP in str. radiatum, aligned to the onset of the UP state, showed a dominance of gamma power associated with the cortical DOWN state. In contrast, gamma activity in the dentate gyrus and str. lacunosum-moleculare was invariably larger during the UP state of entorhinal cortical cells (Figure 7B). To quantify the effect of slow oscillations on the intrahippocampal network activity, we computed the coherence between the membrane potential of entorhinal cells and the instantaneous gamma power (20–60 Hz) in the hippocampus. As in the behaving rat (Bragin et al., 1995), average gamma frequency power increased with depth in the CA1-dentate axis and also exhibited power fluctuations at slow oscillation frequency (Figures 7E and 7G). Coherence and phase shift between gamma power of the LFP and intracellular membrane potential varied differentially and significantly across hippocampal layers (Figures 7F, 7H, and 7I; n = 14 rats). Coherence values were highest in str. lacunosum-moleculare, the molecular layer, and the CA1 pyramidal layer and lowest in str. radiatum. In addition, the phase shift between gamma power and slow oscillation depended on the recording site and was larger in str. radiatum than in other layers (Figures 7F and 7I and Figure S7). These observations, combined with phase-shifted dominant activity of CA3 neurons (Figure 5), suggest that the CA3 circuit can generate self-organized gamma oscillations independent of cortical-entorhinal inputs, whereas gamma activity in the dentate gyrus is entorhinal input dependent.

Similar observations were made in naturally sleeping rats (n = 4 rats). Gamma power in the entorhinal cortex, dentate gyrus, and CA1 region correlated strongly with the UP state. In accordance with the enhanced activity of CA3 neurons during neocortical delta waves (Figure 6A), gamma oscillation trains confined to CA1 str. radiatum were often observed during the DOWN state (Figures 7C and 7D). The main difference between

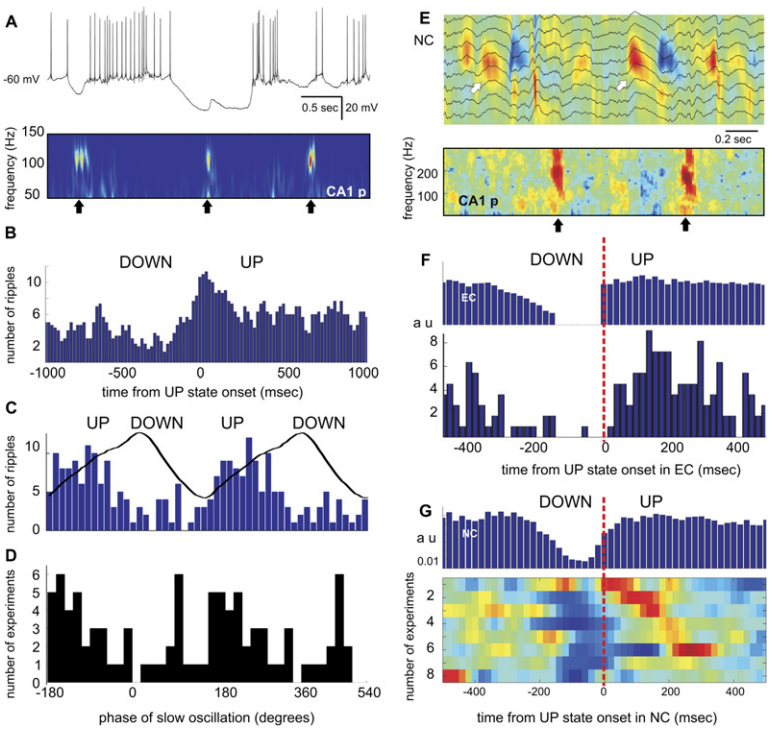

Figure 8. Relationship between Slow Oscillation and Hippocampal Sharp Wave/Ripple Complex

(A) Example of activity in a layer 3 entorhinal neuron and associated spectrogram of LFP in CA1 pyramidal layer. Arrows, ripples. Note transient depolarizations during both DOWN and UP states after ripples.

(B) Temporal distribution of ripple occurrence relative to DOWN-UP transition (0 ms) of the membrane potential in layer 2 and 3 entorhinal neurons (n = 8). Note increased ripple occurrence in the UP state.

(C) Distribution of ripple occurrences as a function of phase of neocortical slow oscillation in LFP in a representative experiment.

(D) Distribution of preferred phases of ripples across experiments with significant modulation of ripples occurrence by the slow oscillation (n = 46 of 137 experiments).

(E–G) Data from naturally sleeping rats. (E) Example of neocortical delta waves (white arrows; LFP traces and CSD map) and associated spectrogram of LFP in CA1 pyramidal layer. Black arrows, ripples. (F) Relationship between DOWN-UP transition of population firing in the entorhinal cortex (EC, top) and the occurrence of hippocampal ripples (bottom). (G) Relationship between DOWN-UP transition of population firing in the neocortex (NC, top) and the occurrence of hippocampal ripples (bottom). Each line is a color-coded cross-correlogram (8 sessions, 7 rats).

sleeping and anesthetized animals was the higher frequency of gamma oscillation in the sleeping animal (compare Figures 7B and 7D).

Slow Oscillation Biases Ripple Generation

In addition to gamma oscillations, the CA3-CA1 region also gives rise to the most synchronous hippocampal pattern, the sharp wave-ripple complex (Buzsaki, 1996; Chrobak and Buzsaki, 1996), although at a significantly reduced rate in the anesthetized rat compared to the drug-free animal (Ylinen et al., 1995). Ripples occurred mostly in the UP state of the slow oscillation and were robustly correlated with the discharge of CA1 neurons. Ripples that occurred in the DOWN state evoked transient, large depolarizations and spiking in subicular and entorhinal neurons, after which the membrane potential reverted to the DOWN state (Figure 8A). Thus, ripple-associated synchronous hippocampal-subicular-entorhinal outputs does not cause a global DOWN-UP shift in neocortical networks. The sharp wave-ripple complex associated hippocampal output was effective, however, in depolarizing target neurons, whereas the output associated with gamma episodes was not (n = 5; Figure S8). Analysis of the relationship of ripple occurrence relative to the time of DOWN-UP transition of the superficial entorhinal neurons (Figure 8B) and phase of the slow oscillation (Figures 8C and 8D) revealed that the lowest probability of ripple occurrence coincided with the onset of cortical DOWN state and increased to higher levels after the DOWN-UP transition, marked by the trough of the slow oscillation LFP. Observations in naturally sleeping animals corroborated these findings. At the group level, most ripples occurred during the UP state, particularly at ~100 ms after the entorhinal DOWN-UP transition and ~200 ms after the neocortical DOWN-UP shift (Figures 8E and 8F). Thus, although the sharp wave-ripple complex is a genuine intrahippocampal event (Buzsaki, 1996; Kubota et al., 2003), its occurrence can be temporally biased by the phase transition of neocortical networks from silence to activity (Sirota et al., 2003).

Discussion

During delta waves of sleep and slow oscillations of anesthesia, most neuronal activity in the neocortex becomes synchronously and periodically silent (Steriade et al., 1993c; Achermann and Borbely, 1997). Our findings extend these observations by showing that the paleocortical, entorhinal, and subicular structures and the dentate gyrus of the hippocampus are integral parts of this transient quiescence. Although the CA3 and CA1 network can sustain organized patterns independent of the neocortex (DOWN state), activity of their neurons is biased temporally by the slow oscillations.

Periodic Reset of Neocortical-Paleocortical-Hippocampal Activity

A remarkable feature of slow oscillation is the synchrony over large cortical areas (Amzica and Steriade, 1995; Destexhe et al., 1999; Battaglia et al., 2004). Our findings show that slow oscillation-related alternation of activity and silence expands from the prefrontal cortex to the hippocampal dentate gyrus and can also affect the CA3 and CA1 regions. The simplest explanation of synchronous activity over such a large cortical territory is to assume a common drive from a shared input. For example, inputs from the basal forebrain or brainstem

whose neurons discharge in phase with the slow oscillation (Detari et al., 1997; Lestienne et al., 1997; Duque et al., 2000) can pace widely distributed areas of the cerebral cortex. An alternative common drive to the cortex involves the thalamus, because thalamic neurons also display UP-DOWN bistability (Hughes et al., 2002), timed by the corticothalamic inputs (Steriade et al., 1993a). However, the common drive hypothesis cannot fully account for our observations that CA3 and CA1 neurons were also active during the neocortical-paleocortical DOWN states. In addition, the sparsity of thalamic projection to the entorhinal cortex, subiculum, and hippocampus (Amaral and Witter, 1989) further limits the critical role of the thalamus in slow oscillations. Finally, the common drive hypothesis cannot simply explain the fronto-caudal spread of the slow oscillation, demonstrated in the human brain (Massimini et al., 2004) and the time shift between neocortical and dentate oscillations shown here. Alternatively, slow oscillations arise in the recurrent local circuits of deep cortical layers (Sanchez-Vives and McCormick, 2000; Huber et al., 2004; Luczak et al., 2006), and the widespread synchrony is brought about by long-range cortical connections originating in superficial cortical layers (Amzica and Steriade, 1995; Sporns et al., 2000; Shu et al., 2003). The importance of the superficial pathways is supported by our experiments. Both layer 2 and 3 entorhinal inputs to the hippocampal formation produced large sinks and gamma oscillations in the dentate molecular layer and str. lacunosum-moleculare and discharged a portion of the target neurons. Therefore, we hypothesize that in the intact brain the excitatory front of slow oscillation spreads from the neocortex to the hippocampus by way of the entorhinal cortex.

Defining features of the slow oscillation are the abrupt shifts of the membrane potential at the neuronal level and the periodic alternation of activity and silence at the network level (Steriade et al., 1993b; Shu et al., 2003). Extensive recurrent collaterals and balanced excitation and inhibition have been hypothesized to be the major requirements for the persistence of the UP state (Steriade et al., 1993b; Sanchez-Vives and McCormick, 2000; Hasenstaub et al., 2005), whereas the DOWN state is thought to be brought about by activity-induced intrinsic conductances and/or the metabolic constraints of the Na/K-ATPase pump (Cowan and Wilson, 1994; Wilson and Kawaguchi, 1996; Cunningham et al., 2006). Our findings imply that these necessary conditions for the UP state may not be sufficient for the maintenance of slow oscillations because recurrent collateral excitation and balanced inhibition and excitation are also present in the hippocampus, yet hippocampal neurons did not show bimodal distribution of their membrane potential. Instead, they were either driven by the excitatory entorhinal volleys or generated intrinsic gamma or ripple oscillations without robust bistable shifts in the membrane potential, indicating that hitherto not well-understood differences exist between neo/paleocortical and hippocampal neurons and networks. Recently, it has been suggested that the hippocampus gives rise to an independent slow oscillation because alternating sinks and associated unit discharges were observed in the hippocampus, concurrent with neocortical slow oscillations (Wolansky et al., 2006). Our findings are at odds with this interpretation and indicate instead that slow oscillations arise in neo- and paleocortical circuits, which impose their outputs on the hippocampal networks. From the perspective of dynamical systems, synchronization by slow oscillations within and between networks can be explained by coherence resonance. In this formulation, coupled linear (bistable) networks engage into synchronized oscillatory dynamics at an "optimum" level of noise. The different network size or connectivity of the hippocampus may prevent it from generating slow oscillations on its own (Pikovsky et al., 2001), yet its activity can be paced by the neo/paleocortical inputs.

Hippocampal Subregions Can Generate Independent Activity Patterns

Although the hippocampal formation is generally thought of as a feedforward excitatory path through which coordinated patterns are propelled from the dentate gyrus to the CA1-subicular output regions (Amaral and Witter, 1989), our findings indicate that hippocampal subregions cooperate differently under various conditions. Nearly all dentate gyrus and the majority of CA1 neurons fired preferentially in the UP state concurrent with increased gamma frequency oscillations in the dentate molecular layer and CA1 str. lacunosum-moleculare. This slow oscillation-related "resetting" of hippocampal activity is similar to the periodic decrease of hippocampal unit discharges at the onset of neocortical delta waves in naturally sleeping rodents (Sirota et al., 2003; Moelle et al., 2006). CA1 neurons active in the UP state might have been driven by either the direct layer 3 entorhinal input (Charpak et al., 1995) or the trisynaptic intrahippocampal path. In the DOWN state, two types of self-organized patterns were present: gamma oscillations and ripples. Previous work in vitro has shown that, under the right pharmacological conditions, gamma oscillations and ripples depend on the CA3 recurrent collateral system (Fisahn et al., 1998; Kubota et al., 2003; Maier et al., 2003). Furthermore, surgical removal of the entorhinal cortex enhances the power of gamma oscillations in the CA3-CA1 regions and increases the incidence of ripple events (Bragin et al., 1995). However, the conditions that determine the switch between gamma oscillations and sharp wave-ripples remain to be explored.

In the naturally sleeping animal, gamma and ripple oscillations in the DOWN state were less dominant perhaps because the short duration of DOWN states associated with delta waves may have limited the emergence of these self-organized patterns. Ripples that emerge in the DOWN state may "replay" stored information within hippocampal circuits and selectively modify intrahippocampal, subicular, and entorhinal cortical connectivity without affecting neocortical targets. Alternatively, ripples associated with the DOWN state may reflect a "correcting" mechanism by eliminating functional pathways no longer needed for hippocampal neocortical information transfer. Independent of these speculations, our findings suggest that the dentate gyrus output can affect the CA3 targets in two different ways. In the UP state, granule cells firing at gamma frequency transmit neocortical information by their potentiating excitatory mossy terminals onto a few selected pyramidal neurons (Henze et al., 2002) while at the same time suppress the

remaining CA3 population by widespread activation of inhibitory neurons (Acsady et al., 1998). In the DOWN state, the absence of the dentate-mediated suppression allows for the occurrence of transient self-organized gamma and sharp wave/ripple oscillations in the CA3-CA1 circuits. Thus, the hippocampus proper can operate in both neo/paleocortex-dependent and independent manner. These observations indicate that although hippocampal ripples and gamma oscillations can emerge as self-organized patterns, their probability of occurrence and the constitution of the participating neurons in these events may be biased by the state of the neocortex.

Temporal Coordination of Neocortical-Hippocampal Transfer of Neuronal Patterns

The periodic "rebooting" of activity in the neocortical, entorhinal, and hippocampal axis provides a framework for a temporally coordinated communication in these circuits during sleep. It has been hypothesized that experience-related activity modifies synaptic strengths of functional connectivity among the neurons involved and that episodic memory traces embodied in the modified connectivity undergo further modification during sleep (Wilson and McNaughton, 1994; Hasselmo et al., 1995; Buzsaki, 1996; Csicsvari et al., 2000). An important physiological role of slow oscillations is the temporal coordination of locally emerging patterns, such as sleep spindles, gamma oscillations (Steriade et al., 1993c), and sharp wave-ripple events, and their ability to affect the direction of activity spread by phase offset over large cortical areas. After each DOWN state, the neocortex self-organizes its global activity from locally generated patterns (Luczak et al., 2006). Because the spatiotemporal sequences of neocortical neurons during the UP state recur reliably in successive episodes (Luczak et al., 2006), we hypothesize that the output of neocortical patterns can select unique subpopulations of hippocampal neurons. In turn, the targeted hippocampal neurons give rise to ripple-related synchronous outputs back to the still active neocortical assemblies (Chrobak and Buzsaki, 1996). The temporal directedness of these events facilitates conditions in which unique neocortical inputs to the hippocampus and hippocampal outputs to the neocortex may be selectively modified (Sirota et al., 2003). Direct support of this hypothetical mechanism will require demonstration that specific assemblies in the neocortex-entorhinal cortex-hippocampus axis during sleep are brought about by waking experience.

Experimental Procedures

Animal Surgery

For acute experiments, 218 male Sprague-Dawley rats (140–250 g; Hilltop Laboratories) were anesthetized with urethane only (1.5 g/kg, i.p.) or urethane (1.25 g/kg, i.p.) plus additional ketamine/xylazine injections (20 and 2 mg/kg I.M. for maintenance). Data from several of these animals were used in previous studies (Harris et al., 2000; Henze et al., 2000). The body temperature was monitored and kept constant with a heating pad. The head was placed in a stereotaxic frame, the skull was exposed, and a small hole (1.2 mm in diameter) in the skull was drilled above the hippocampus (A, −4.5 mm from the bregma; L, 5.0 mm from the midline; D, 2.0–2.2 mm from brain surface) to insert an extracellular electrode at a 15° angle toward the midline. Another hole in the skull was drilled above the ipsilateral prefrontal cortex (A, 3.0; L, 0.5–1.0), the somatosensory cortex/hippocampus (A, −3.5; L, 2.5), or occipital cortex/entorhinal cortex (A, lambda; L, 5.0) to insert an intracellular electrode vertically. Two miniature stainless-steel screws were driven into the skull and served as ground and reference electrodes, respectively, for extracellular recording. An Ag-AgCl wire was placed in the neck as a reference electrode for intracellular recording. The bone holes were covered with paraffin wax after electrode insertion (Henze et al., 2000). For chronic surgery, nine Long Evans rats (male, 250–400 g) were deeply anesthetized with isoflurane. The rest of the surgery and recovery procedures are described in detail elsewhere (Csicsvari et al., 2003). All experiments were carried out in accordance with protocols approved by the Rutgers University Animal Care and Use Committee.

Electrophysiological Methods

Extracellular signal was amplified and filtered by a multichannel AC amplifier (Sensorium EPA5 or RC Electronics; 1000×; 1 Hz to 5 kHz). The intracellular signals were amplified with a DC amplifier (Axoprobe 1A; Axon Instruments). Wide-band extracellular and intracellular signals were digitized at 20 or 25 kHz and stored for offline analysis (DataMax System 64; RC Electronics, Santa Barbara, CA). In acute experiments, recordings were done using a single tetrode (four 12.5 μm diameter nichrome wires) or silicon probes (Henze et al., 2000) placed in the CA1 pyramidal layer, layer 5 of the prefrontal cortex or the entorhinal cortex. In 17 rats, a single-shank 16 site (at 100 μm intervals) silicon probe placed in the CA1-dentate gyrus axis (NeuroNexus Technologies). Online positioning of the electrodes was assisted by the presence of unit activity and fast oscillatory field ("ripple") activity in the CA1 pyramidal layer and by the characteristic distribution of evoked potentials in response to angular bundle stimulation (single pulses 25–100 μA, 0.1 ms). Only 14 experiments with appropriate position of the probe were used for analysis. Intracellular penetrations were carried out with sharp glass capillaries, pulled from borosilicate glass tubes and filled with 1 M K-acetate and 2% biocytin (pH 7.4, 40–68 MΩ). After the membrane potential became stable, brief hyperpolarizing and depolarizing currents were injected through the electrode to characterize membrane potential properties (+0.1–0.5 nA, 500 ms). Only healthy neurons (input resistance >20 MΩ; resting membrane potential <−55 mV; with overshooting action potentials) were accepted for further recordings. At the end of the physiological data collection, biocytin was loaded into the recorded neuron by positive current pulses (+0.5–0.8 nA, 500 ms at 1 Hz, 5–60 min).

In chronic experiments nine rats were implanted with a microdrive that allowed the positioning of recording electrodes in the dorsal-medial entorhinal cortex (n = 1, Hafting et al., 2005) or somatosensory/parietal cortex and the dorsal hippocampus (CA1 or CA3b-dentate area; n = 8 rats). Various silicon probes were used for recording: high-density 4-shank "octrode," 32-site probes (n = 1; Csicsvari et al., 2003; Bartho et al., 2004), 16-site linear probes (n = 5; Sirota et al., 2003), and 6-shank 96-site linear probes (n = 3, Csicsvari et al., 2003) for simultaneous recording of unit activity and field potentials in different cortical layers and/or hippocampus. The position of the electrodes was confirmed histologically.

Histology

Under deep urethane anesthesia, the animals were perfused intracardially with 100 ml cold saline followed by 250–300 ml of 10% formalin or 4% paraformaldehyde and 0.5% glutaraldehyde in 0.1 M phosphate buffer (pH = 7.4). The brains were removed and postfixed at 4°C overnight and then sliced into 50 μm thick coronal (neocortex and hippocampus) parasaggital (subiculum) or horizontal (entorhinal cortex) sections. The biocytin-loaded neurons were labeled by the avidin-biotin-HRP complex method with diaminobenzidine and nickel. After thionin counterstaining, the labeled neurons were reconstructed with a NeuroLucida, together with the tracks of the extracellular electrodes. In the somatosensory cortex, only a fraction of neurons were stained and therefore no layer assignment is shown for these cells.

Data Analysis

Raw data were preprocessed using a custom-developed suite of programs (Csicsvari et al., 1999). Wide-band signal was downsampled to 1250 Hz and used as local field potential signal. For spike detection, wide-band signal was high-pass filtered (>0.8 kHz). Single units were isolated semiautomatically by a custom-developed

clustering analysis program KlustaKwik (http://sourceforge.net/projects/klustakwik/) (Harris et al., 2000) and refined manually using custom-made software (http://klusters.sourceforge.net; http://neuroscope.sourceforge.net; Hazan et al., 2006). Local field potentials, extracellular units, and intracellular data were analyzed by custom-written, MATLAB-based programs. For all the analysis, only periods containing slow oscillations were used (Figure S1). Spectral analyses were carried out using direct multi-taper estimate (Mitra and Pesaran, 1999) or continuous wavelet transformation (Torrence and Compo, 1998). The parameters of the spectral estimate varied depending on the frequency range. Sharp wave-associated fast oscillations (ripples) in CA1 pyramidal layer were detected as described earlier (Csicsvari et al., 2000). Instantaneous gamma power was computed in sliding 200 ms windows and was used as a signal for spectral analysis in the slow oscillation frequency range (e.g., Figure 7). Coherence between the intracellular membrane potential and instantaneous LFP gamma power at each recording site was computed and depth profile of high coherence consistent across experiments was extracted by principal component analysis. The eigenvectors corresponding to two largest eigenvalues identified depth profiles of largest covariance of the synaptic currents across experiments. For phase analysis, the LFP recorded in the CA1 pyramidal layer was filtered for slow oscillations (adjusted for each cell; typically ~1 Hz), and the instantaneous phase was computed as the angle of the Hilbert transformation of the filtered signal. Phase modulation of spikes and ripples was determined by Rayleigh circular statistics (Fisher, 1993); $p < 0.05$ was considered significant. For all circular statistical tests the nonuniformity of the phase distribution, due to skewness of the slow oscillation wave shape, was taken into account using the cumulative density function-based transformation (Siapas et al., 2005). Group comparison tests of circular variables were performed using circular ANOVA.

Current-source density (CSD) analysis of the simultaneously recorded field potentials was used to eliminate volume conduction and localize synaptic currents. CSD was computed for each recording site according to differential scheme for second derivative and smoothed with a triangular kernel (Freeman and Nicholson, 1975). Location of the recording electrode sites in the hippocampus was determined by computing CSD of sharp waves and evoked potentials in response to perforant path or commissural path stimulation (see Figure 4) (Bragin et al., 1995). In all analyses of the membrane potential signals, an average of the intracellular action potential was computed for each cell, and the membrane potential was interpolated for the duration of the spike (typically ~3 ms). Spectral power of the membrane potential was computed, and the relative power coefficient (ratio of the peak power and the standard deviation across all frequencies) was used to characterize the strength of the dominant frequency of slow oscillation. For further details, see Supplementary Data.

Supplemental Data

The Supplemental Data for this article can be found online at http://www.neuron.org/cgi/content/full/52/5/871/DC1/.

Acknowledgments

We thank A. Amarasingham, D.A. McCormick, D. Paré, A. Renart, D. Robbe, D. Sullivan, J.M. Tepper, and L. Záborszky for their support and comments. We dedicate this paper to the late Mircea Steriade. Supported by National Institutes of Health (NS043157, 034994; MH54671 to G.B.), Uehara Memorial Foundation, and the Japan Society of Promotion for Sciences (to Y.I. and K.M.).

Received: June 7, 2006
Revised: September 28, 2006
Accepted: October 24, 2006
Published: December 6, 2006

References

Achermann, P., and Borbely, A.A. (1997). Low-frequency (< 1 Hz) oscillations in the human sleep electroencephalogram. Neuroscience *81*, 213–222.

Acsády, L., Kamondi, A., Sik, A., Freund, T., and Buzsáki, G. (1998). GABAergic cells are the major postsynaptic targets of mossy fibers in the rat hippocampus. J. Neurosci. *18*, 3386–3403.

Amaral, D.G., and Witter, M.P. (1989). The three-dimensional organization of the hippocampal formation: a review of anatomical data. Neuroscience *31*, 571–591.

Amzica, F., and Steriade, M. (1995). Disconnection of intracortical synaptic linkages disrupts synchronization of a slow oscillation. J. Neurosci. *15*, 4658–4677.

Barthó, P., Hirase, H., Monconduit, L., Zugaro, M., Harris, K.D., and Buzsáki, G. (2004). Characterization of neocortical principal cells and interneurons by network interactions and extracellular features. J. Neurophysiol. *92*, 600–608.

Battaglia, F.P., Sutherland, G.R., and McNaughton, B.L. (2004). Hippocampal sharp wave bursts coincide with neocortical "up-state" transitions. Learn. Mem. *11*, 697–704.

Bragin, A., Jandó, G., Nadásdy, Z., Hetke, J., Wise, K., and Buzsáki, G. (1995). Gamma (40-100 Hz) oscillation in the hippocampus of the behaving rat. J. Neurosci. *15*, 47–60.

Buzsáki, G. (1996). The hippocampo-neocortical dialogue. Cereb. Cortex *6*, 81–92.

Buzsáki, G., and Draguhn, A. (2004). Neuronal oscillations in cortical networks. Science *304*, 1926–1929.

Buzsáki, G., Horváth, Z., Urioste, R., Hetke, J., and Wise, K. (1992). High-frequency network oscillation in the hippocampus. Science *256*, 1025–1027.

Charpak, S., Paré, D., and Llinás, R. (1995). The entorhinal cortex entrains fast CA1 hippocampal oscillations in the anaesthetized guinea-pig: role of the monosynaptic component of the perforant path. Eur. J. Neurosci. *7*, 1548–1557.

Chrobak, J.J., and Buzsáki, G. (1996). High-frequency oscillations in the output networks of the hippocampal-entorhinal axis of the freely behaving rat. J. Neurosci. *16*, 3056–3066.

Cowan, R.L., and Wilson, C.J. (1994). Spontaneous firing patterns and axonal projections of single corticostriatal neurons in the rat medial agranular cortex. J. Neurophysiol. *71*, 17–32.

Csicsvari, J., Hirase, H., Czurko, A., Mamiya, A., and Buzsáki, G. (1999). Oscillatory coupling of hippocampal pyramidal cells and interneurons in the behaving Rat. J. Neurosci. *19*, 274–287.

Csicsvari, J., Hirase, H., Mamiya, A., and Buzsáki, G. (2000). Ensemble patterns of hippocampal CA3-CA1 neurons during sharp wave-associated population events. Neuron *28*, 585–594.

Csicsvari, J., Henze, D.A., Jamieson, B., Harris, K.D., Sirota, A., Barthó, P., Wise, K.D., and Buzsáki, G. (2003). Massively parallel recording of unit and local field potentials with silicon-based electrodes. J. Neurophysiol. *90*, 1314–1323.

Cunningham, M.O., Pervouchine, D.D., Racca, C., Kopell, N.J., Davies, C.H., Jones, R.S., Traub, R.D., and Whittington, M.A. (2006). Neuronal metabolism governs cortical network response state. Proc. Natl. Acad. Sci. USA *103*, 5597–5601.

Destexhe, A., Contreras, D., and Steriade, M. (1999). Spatiotemporal analysis of local field potentials and unit discharges in cat cerebral cortex during natural wake and sleep states. J. Neurosci. *19*, 4595–4608.

Détári, L., Rasmusson, D.D., and Semba, K. (1997). Phasic relationship between the activity of basal forebrain neurons and cortical EEG in urethane-anesthetized rat. Brain Res. *759*, 112–121.

Dickson, C.T., Biella, G., and de Curtis, M. (2003). Slow periodic events and their transition to gamma oscillations in the entorhinal cortex of the isolated Guinea pig brain. J. Neurophysiol. *90*, 39–46.

Duque, A., Balatoni, B., Détári, L., and Záborszky, L. (2000). EEG correlation of the discharge properties of identified neurons in the basal forebrain. J. Neurophysiol. *84*, 1627–1635.

Fisahn, A., Pike, F.G., Buhl, E.H., and Paulsen, O. (1998). Cholinergic induction of network oscillations at 40 Hz in the hippocampus in vitro. Nature *394*, 186–189.

Fisher, N.I. (1993). Statistical Analysis of Circular Data (New York: Cambridge University Press).

Freeman, J.A., and Nicholson, C. (1975). Experimental optimization of current source-density technique for anuran cerebellum. J. Neurophysiol. *38*, 369–382.

Friston, K.J. (2000). The labile brain. I. Neuronal transients and nonlinear coupling. Philos. Trans. R. Soc. Lond. B Biol. Sci. *355*, 215–236.

Hafting, T., Fyhn, M., Molden, S., Moser, M.B., and Moser, E.I. (2005). Microstructure of a spatial map in the entorhinal cortex. Nature *436*, 801–806.

Harris, K.D., Henze, D.A., Csicsvari, J., Hirase, H., and Buzsáki, G. (2000). Accuracy of tetrode spike separation as determined by simultaneous intracellular and extracellular measurements. J. Neurophysiol. *84*, 401–414.

Hasenstaub, A., Shu, Y., Haider, B., Kraushaar, U., Duque, A., and McCormick, D.A. (2005). Inhibitory postsynaptic potentials carry synchronized frequency information in active cortical networks. Neuron *47*, 423–435.

Hasselmo, M.E., Schnell, E., and Barkai, E. (1995). Dynamics of learning and recall at excitatory recurrent synapses and cholinergic modulation in rat hippocampal region CA3. J. Neurosci. *15*, 5249–5262.

Hazan, L., Zugaro, M., and Buzsáki, G. (2006). Klusters, NeuroScope, NDManager: A free software suite for neurophysiological data processing and visualization. J. Neurosci. Methods *155*, 207–216.

Henze, D.A., Borhegyi, Z., Csicsvari, J., Mamiya, A., Harris, K.D., and Buzsáki, G. (2000). Intracellular features predicted by extracellular recordings in the hippocampus in vivo. J. Neurophysiol. *84*, 390–400.

Henze, D.A., Wittner, L., and Buzsáki, G. (2002). Single granule cells reliably discharge targets in the hippocampal CA3 network in vivo. Nat. Neurosci. *5*, 790–795.

Huber, R., Ghilardi, M.F., Massimini, M., and Tononi, G. (2004). Local sleep and learning. Nature *430*, 78–81.

Hughes, S.W., Cope, D.W., Blethyn, K.L., and Crunelli, V. (2002). Cellular mechanisms of the slow (<1 Hz) oscillation in thalamocortical neurons in vitro. Neuron *33*, 947–958.

Kloosterman, F. (2003). PhD thesis, University of Amsterdam, Amsterdam.

Kubota, D., Colgin, L.L., Casale, M., Brucher, F.A., and Lynch, G. (2003). Endogenous waves in hippocampal slices. J. Neurophysiol. *89*, 81–89.

Lestienne, R., Herve-Minvielle, A., Robinson, D., Briois, L., and Sara, S.J. (1997). Slow oscillations as a probe of the dynamics of the locus coeruleus-frontal cortex interaction in anesthetized rats. J. Physiol. (Paris) *91*, 273–284.

Luczak, A., Barthó, P., Marguet, S.L., Buzsáki, G., and Harris, K.D. (2006). Neocortical spontaneous activity in vivo: cellular heterogeneity and sequential structure. Proc. Natl. Acad. Sci. USA, in press.

MacLean, P. (1990). The Triune Brain in Evolution: Role in Paleocerebral Functions (New York: Plenum Press).

Maier, N., Nimmrich, V., and Draguhn, A. (2003). Cellular and network mechanisms underlying spontaneous sharp wave-ripple complexes in mouse hippocampal slices. J. Physiol. *550*, 873–887.

Massimini, M., Huber, R., Ferrarelli, F., Hill, S., and Tononi, G. (2004). The sleep slow oscillation as a traveling wave. J. Neurosci. *24*, 6862–6870.

McCormick, D.A. (1992). Neurotransmitter actions in the thalamus and cerebral cortex and their role in neuromodulation of thalamocortical activity. Prog. Neurobiol. *39*, 337–388.

McCormick, D.A., Shu, Y., Hasenstaub, A., Sanchez-Vives, M., Badoual, M., and Bal, T. (2003). Persistent cortical activity: mechanisms of generation and effects on neuronal excitability. Cereb. Cortex *13*, 1219–1231.

Mitra, P.P., and Pesaran, B. (1999). Analysis of dynamic brain imaging data. Biophys. J. *76*, 691–708.

Moelle, M., Yeshenko, O., Marshall, L., Sara, S.J., and Born, J. (2006). Hippocampal sharp wave-ripples linked to slow oscillations in rat slow-wave sleep. J. Neurophysiol. *96*, 62–70.

Mukovski, M., Chauvette, S., Timofeev, I., and Volgushev, M. (2006). Detection of active and silent states in neocortical neurons from the field potential signal during slow-wave sleep. Cereb Cortex., in press. Published online March 17, 2006. 10.1093/cercor/bhj157.

Pelletier, J.G., Apergis, J., and Paré, D. (2004). Low-probability transmission of neocortical and entorhinal impulses through the perirhinal cortex. J. Neurophysiol. *91*, 2079–2089.

Petersen, C.C., Hahn, T.T., Mehta, M., Grinvald, A., and Sakmann, B. (2003). Interaction of sensory responses with spontaneous depolarization in layer 2/3 barrel cortex. Proc. Natl. Acad. Sci. USA *100*, 13638–13643.

Pikovsky, A., Rosenblum, M., and Kurth, J. (2001). Synchronization: A Universal Concept in Nonlinear Dynamics (Cambridge: Cambridge University Press).

Sanchez-Vives, M.V., and McCormick, D.A. (2000). Cellular and network mechanisms of rhythmic recurrent activity in neocortex. Nat. Neurosci. *3*, 1027–1034.

Shu, Y., Hasenstaub, A., and McCormick, D.A. (2003). Turning on and off recurrent balanced cortical activity. Nature *423*, 288–293.

Siapas, A.G., and Wilson, M.A. (1998). Coordinated interactions between hippocampal ripples and cortical spindles during slow-wave sleep. Neuron *21*, 1123–1128.

Siapas, A.G., Lubenov, E.V., and Wilson, M.A. (2005). Prefrontal phase locking to hippocampal theta oscillations. Neuron *46*, 141–151.

Sirota, A., Csicsvari, J., Buhl, D., and Buzsáki, G. (2003). Communication between neocortex and hippocampus during sleep in rodents. Proc. Natl. Acad. Sci. USA *100*, 2065–2069.

Sporns, O., Tononi, G., and Edelman, G.M. (2000). Connectivity and complexity: the relationship between neuroanatomy and brain dynamics. Neural Netw. *13*, 909–922.

Steriade, M., and Buzsáki, G. (1990). Parallel activation of thalamic and cortical neurons by brainstem and basal forebrain cholinergic systems. In Brain Cholinergic Systems, M. Steriade and D. Biesold, eds. (Oxford: Oxford University Press), pp. 3–64.

Steriade, M., Contreras, D., Curro, D.R., and Nuñez, A. (1993a). The slow (< 1 Hz) oscillation in reticular thalamic and thalamocortical neurons: scenario of sleep rhythm generation in interacting thalamic and neocortical networks. J. Neurosci. *13*, 3284–3299.

Steriade, M., Nuñez, A., and Amzica, F. (1993b). A novel slow (< 1 Hz) oscillation of neocortical neurons in vivo: depolarizing and hyperpolarizing components. J. Neurosci. *13*, 3252–3265.

Steriade, M., Nuñez, A., and Amzica, F. (1993c). Intracellular analysis of relations between the slow (< 1 Hz) neocortical oscillation and other sleep rhythms of the electroencephalogram. J. Neurosci. *13*, 3266–3283.

Timofeev, I., Grenier, F., and Steriade, M. (2000). Impact of intrinsic properties and synaptic factors on the activity of neocortical networks in vivo. J. Physiol. (Paris) *94*, 343–355.

Timofeev, I., Grenier, F., and Steriade, M. (2001). Disfacilitation and active inhibition in the neocortex during the natural sleep-wake cycle: an intracellular study. Proc. Natl. Acad. Sci. USA *98*, 1924–1929.

Torrence, C., and Compo, G.P. (1998). A Practical guide to wavelet analysis. Bull. Amer. Meteor. Soc. *79*, 61–78.

Wilson, C.J., and Kawaguchi, Y. (1996). The origins of two-state spontaneous membrane potential fluctuations of neostriatal spiny neurons. J. Neurosci. *16*, 2397–2410.

Wilson, M.A., and McNaughton, B.L. (1994). Reactivation of hippocampal ensemble memories during sleep. Science *265*, 676–679.

Wolansky, T., Clement, E.A., Peters, S.R., Palczak, M.A., and Dickson, C.T. (2006). Hippocampal slow oscillation: a novel EEG state and its coordination with ongoing neocortical activity. J. Neurosci. *26*, 6213–6229.

Ylinen, A., Bragin, A., Nadásdy, Z., Jandó, G., Szabó, I., Sik, A., and Buzsáki, G. (1995). Sharp wave-associated high-frequency oscillation (200 Hz) in the intact hippocampus: network and intracellular mechanisms. J. Neurosci. *15*, 30–46.